

*Revealing transitions in friction-excited
vibrations by nonlinear time-series analysis*

**Merten Stender, Mariano Di
Bartolomeo, Francesco Massi & Norbert
Hoffmann**

Nonlinear Dynamics

An International Journal of Nonlinear
Dynamics and Chaos in Engineering
Systems

ISSN 0924-090X
Volume 98
Number 4

Nonlinear Dyn (2019) 98:2613–2630
DOI 10.1007/s11071-019-04987-7

Your article is protected by copyright and all rights are held exclusively by Springer Nature B.V.. This e-offprint is for personal use only and shall not be self-archived in electronic repositories. If you wish to self-archive your article, please use the accepted manuscript version for posting on your own website. You may further deposit the accepted manuscript version in any repository, provided it is only made publicly available 12 months after official publication or later and provided acknowledgement is given to the original source of publication and a link is inserted to the published article on Springer's website. The link must be accompanied by the following text: "The final publication is available at link.springer.com".



Revealing transitions in friction-excited vibrations by nonlinear time-series analysis

Merten Stender · Mariano Di Bartolomeo · Francesco Massi · Norbert Hoffmann

Received: 14 December 2018 / Accepted: 25 April 2019 / Published online: 3 May 2019
 © Springer Nature B.V. 2019

Abstract We study the transitions in friction-induced vibrations (FIV) experimentally. The measurement data stem from a highly sophisticated setup specifically designed to study FIV problems and where the relative motion between the samples is achieved using air bearings and a voice-coil motor. This peculiarity ensures avoiding parasitic vibrations and makes the setup particularly suitable to perform measurements of very low vibration levels. The relative sliding velocity decays along the measurement to zero, which provokes several types of FIV. We employ advanced time-series analysis techniques, such as spectral analysis, attractor reconstruction and recurrence plot analysis to study the dynamical transition from steady sliding to high-frequency FIV and stick-slip vibrations in detail. For different specimens, self-excited vibrations are observed stemming from an instability that is driven by a negative friction-velocity slope characteristic as well as for constant friction values. Prior to instability, it is observed that highly irregular oscillations decay and

most of the vibration energy focuses in a low-frequency mode of the experimental setup. The analysis of the FIV range illustrates a plethora of qualitatively different dynamics that can be detected, characterized and visualized using advanced signal processing. Particularly, we report on period-1 and period-2 limit cycles, quasi-periodic motion, weakly chaotic attractors and different types of stick-slip vibrations. The analysis of transitions between those dynamic regimes reveals beating phenomena, sudden energy exchange between different modes and intermittent dynamics. The results of this study aim to provide a step forward on the application of nonlinear dynamics post-processing tools for identifying and characterizing the different frictional stable and unstable scenarios.

Keywords Friction-induced vibrations · Stick-slip vibrations · Time-series analysis · Dynamic transitions · Chaotic dynamics · Attractor reconstruction

M. Stender (✉) · N. Hoffmann
 Dynamics Group, Hamburg University of Technology,
 Hamburg, Germany
 e-mail: m.stender@tuhh.de

M. Di Bartolomeo · F. Massi
 DIMA, Department of Mechanical and Aerospace
 Engineering, 'La Sapienza' University of Rome, Rome,
 Italy

N. Hoffmann
 Department of Mechanical Engineering, Imperial College
 London, London, United Kingdom

1 Introduction

Friction-induced vibrations (FIV) [1, 2] have been studied extensively in the last decades owing to their crucial impact on the vibrational behavior of engineering structures. Several excitation mechanisms, such as mode-coupling and negative friction-velocity relationship [3, 4], have been identified numerically and experimentally. However, measuring the frictional interface of two mechanical components in contact and its

dynamics remains a major challenge in experimental testings. Not only the friction partners, but also the complete dynamical system affect the stability and vibration characteristics [5]. Hence, structurally secondary design elements, such as mechanical joints, can have crucial impact on the overall dynamics. For instance, it was shown for passenger car brake systems that those mechanical joints represent one of the major sources for damping with high sensitivity and variability to initial conditions [6,7]. Hence, if the friction interface is researched, other structural dynamics, driving motors and other sources of energy and dissipation may strongly affect the FIV.

Recently, an experimental setup has been developed [8] to allow measurements of friction dynamics at high accuracy. The central advantage of this setup is the usage of air bearings and a voice-coil motor, such that the only dry-friction sliding contact is the one between the two specimens under study. Hence, this setup enables to study the FIV with minuscule impact from the geometrical setup boundary conditions and parasitic noise that is typically encountered in experimental setups.

Chaos in friction-excited systems is well-known and has been investigated in the stick-slip regime for long times [9–17]. For instance, Popp and Stelter [18] investigated different discrete analytical models and experimental data from blocks sliding on a moving belt. Period- n limit cycles as well as chaos were found by the authors. Particularly, the intermittency [19] and period-doubling route to chaos were observed in the data using spectral analysis and phase space reconstruction. Pilipchuk et al. [20] studied a numerical and experimental two-degree of freedom brake model sliding on a belt. For a decreasing velocity profile, creep-slip dynamics were observed. Particularly, the authors report on several transitions in multiple frequency oscillations and short bands of chaotic dynamics. In the multiple frequency vibration range, multiple sub-harmonics and higher harmonics were observed. However, transitions and chaos in high-frequency friction-induced vibrations, i.e., in steady sliding without stick-slip effects, in experimental systems have been studied fewer times.

In this work, we study the FIV under a decreasing relative sliding velocity. This is a classical scenario in various engineering systems such as brakes and clutches. Special focus is put on the transition and characterization of qualitatively different dynam-

ics at different stages of the measured vibration signals. Particularly, advanced signal processing methods from nonlinear time-series and recurrence plot analysis are applied. In the research on disk brake system vibrations, lately these techniques allowed to reveal the qualitative character of the FIV from experimental data. In the steady sliding scenario, researchers [21,22] used nonlinear time-series analysis (NTSA) to reconstruct the invariant set, i.e., the *attractor*, from vibration measurements sampled at high rates. Typically, the broad energy spectrum recorded in the steady sliding regime is assigned to stochastic motion. However, these authors showed evidence for deterministic, but chaotic, motion that is exhibiting a positive Lyapunov exponent in the steady sliding regime. In those measurements, the irregularity decreased as high-frequency FIV vibrations, commonly known as *brake squeal*, set in. [23–25] studied this FIV regime using NTSA and recurrence plot analysis (RPA). For experimental and numerical data, the authors were able to find regular periodic, quasi-periodic as well as chaotic dynamics during brake squeal. Hence, the NTSA and RPA techniques represent powerful approaches to gather understanding and novel insights from limited data, i.e., scalar time-series measurements of complex vibrations.

This work illustrates a plethora of dynamical phenomena that were observed during the frictional tests. First, the experimental setup and the testing specimens are introduced. Then, we briefly elaborate on the methods employed to analyze the data. Then, three vibration measurements are studied in detail. Recurrence quantifiers and spectral properties of short signal epochs are used to qualitatively and quantitatively characterize the friction-induced vibrations.

2 Materials and methods

2.1 The experimental setup

The experimental measurements have been performed by means of the TriboAir setup (Fig. 1), a test bench specifically designed to reproduce the relative motion between two samples in frictional contact under specific loading conditions. The setup allows for reproducing and measuring the FIV during frictional contact under well controlled boundary conditions and low noise disturbance. The upper sample 1 is kept fixed, while the lower sample 2 is mounted on a supporting

bar 3, which is connected to a moving base 4 by means of two tri-axial force transducers 5. The moving base can slide, essentially without friction, on two parallel shafts through two couples of air bearings 6. The movement is provided by a linear voice-coil actuator 7 to which the moving base is fixed. The normal load is applied by means of dead weights driven vertically by two air bearings 8, in order to avoid friction forces that could alter the nominal applied contact pressure. The use of air bearings and voice-coil motor (i.e., without contact between the sliding parts) ensures avoiding parasitic vibrations coming from the setup. For these reasons, the TriboAir is particularly appropriate to perform measurements on very low vibration levels. A laser Doppler vibrometer 9 measures the induced vibrations on the face of the upper samples, close to the contact interface (red spot in Fig. 1, at about 1.5 mm from the interface). A detailed description of the setup can be found in [8].

2.2 Boundary conditions and samples

The two sliding samples have a parallelepiped shape ($10 \times 10 \times 10$ mm and $50 \times 20 \times 10$ mm, respectively). The tests are performed applying a constant normal load to the upper sample and a specific displacement law to the lower sample. In particular, for the tests studied in this paper, the normal load is set at 20 N and the displacement law is depicted in Fig. 2. During the test, the following signals are recorded: a) The normal and tangential forces; b) The vibrational velocity close to the contact interface, along the sliding direction; c) The imposed displacement of the moving base. Signals are recorded at sampling rates of $f_s = 100$ kHz. In this work, we focus on the analysis of the block velocity measured close to the interface. Next, the three system configurations are discussed briefly to introduce the raw measurement signals and salient features of the spectral properties. Spe-

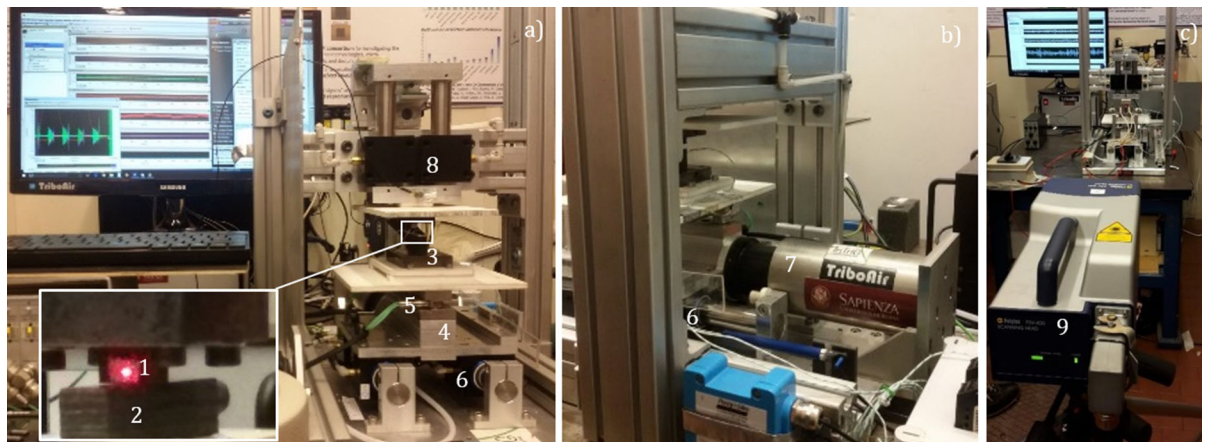


Fig. 1 TriboAir setup: upper sample 1, lower sample 2, supporting bar 3, moving base 4, tri-axial transducers 5, horizontal air bearings 6, Linear voice-coil motor 7, vertical air bearings 8, Laser Doppler Vibrometer 9

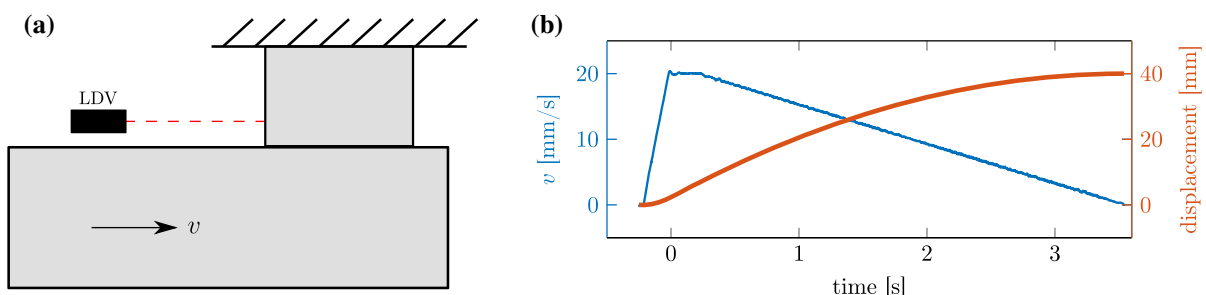


Fig. 2 **a** simplified illustration of the measurement setup and **b** applied displacement (velocity) curve. The lower sample velocity quickly ramps up to 20 mm/s and then decreases linearly to zero at 6 mm/s^2 along time

cific phenomena encountered in those measurements will then be analyzed and discussed in Results section. In the following discussions, the qualitative nature of the observed dynamics is of interest. Hence, the vibration measurements are normalized, denoted as (\cdot) , such that each displayed signal has a unit maximum absolute amplitude.

In this work, systems I, II and III refer to different frictional specimens, selected to show different frictional response. The tested specimens are made of composite carbon/carbon materials generally applied on high-performance brake and clutch systems. This kind of materials is generally composed by a structural matrix made of carbon fibers, fillers and additives. The three sets of specimens used in the three systems have the same structural matrix, i.e., equivalent macroscopic mechanical properties (stiffness, density), but differ in their composition, resulting in different macroscopic friction coefficient and its dependence with contact parameters such as sliding velocity. The different material composition results then in different macroscopic frictional response of the materials as a function of the sliding velocity. In particular, system I presents a negative friction-velocity slope, while system II and III show a constant friction value with respect to the sliding velocity.

2.2.1 System I: negative friction-velocity slope

Figure 3 depicts the raw time-series data recorded for system I. Steady sliding is observed until $t = 2.26$ s, where high-frequency FIV grow due to a negative friction-velocity slope instability. Stick-slip oscillations are marked by two distinct dynamic phases: stick-slip behavior with vanishing motion, sudden braking free and subsequent ring-down-type dynamics observable in the measured velocity time signals. Here, stick-slip oscillations set in at time instant $t = 3.3$ s. The spectral analysis illustrates a rather broad-banded energy distribution in the first regime with pronounced peaks at the 12.08 kHz mode. This mode becomes unstable and oscillates at a slightly lower frequency of 11.9 kHz in the FIV range. Here, two higher harmonics can be observed. Several jumps in the dominant vibration frequency can be observed in the time range $3.19 \leq t \leq 3.3$ s which will be discussed in detail in the following sections.

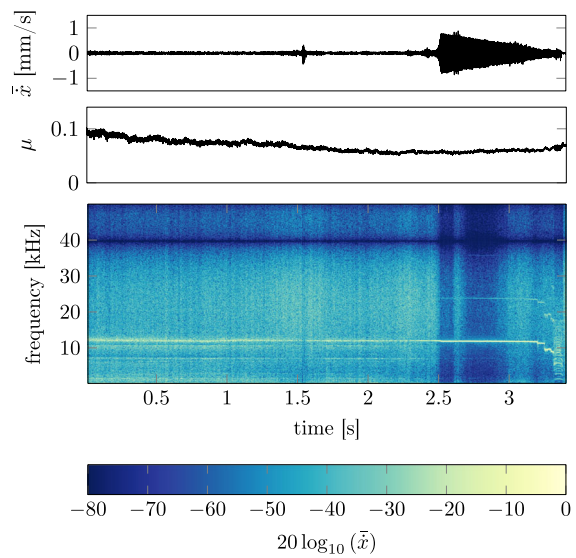


Fig. 3 Recorded time-series data for system I: normalized block velocity \bar{x} , friction coefficient μ and amplitude spectrogram of the velocity signal

2.2.2 System II: constant friction value, no stick-slip oscillations

System II exhibits a constant friction coefficient for the whole test duration. High-frequency FIV set in at $t = 2.33$ s and persists until $t = 3.0$ s, compared to Fig. 4. In this experiment, there were no stick-slip oscillations observed. In the steady sliding regime, at least 7 modes are excited by the friction interface. In the transient growth regime before FIV, beating and spectral scattering phenomena can be observed. The beating stems from an exchange of stability and energy between two modes, which will be elaborated on in the following discussions. In the FIV range, at least 4 harmonics of the base frequency at 5.8 kHz are excited.

2.2.3 System III: piecewise constant friction value

System III exhibits FIV at times $1.56 \leq t \leq 3.3$ s including stick-slip oscillations at low relative sliding velocity. The friction coefficient shows a slight increase prior to FIV onset, as shown in Fig. 5 and then remains constant throughout the vibration duration. The spectrogram exhibits broad energy shares over the complete frequency range, also in the FIV regime. At $t = 2.95$ s and $t = 3.01$ s, abrupt transitions can be observed that are accompanied by jumps in the vibration frequency

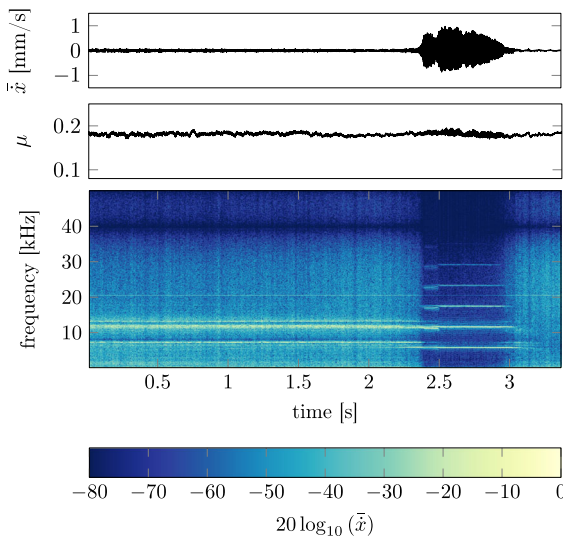


Fig. 4 Recorded time-series data for system II: normalized block velocity \bar{x} , friction coefficient μ and amplitude spectrogram of the velocity signal

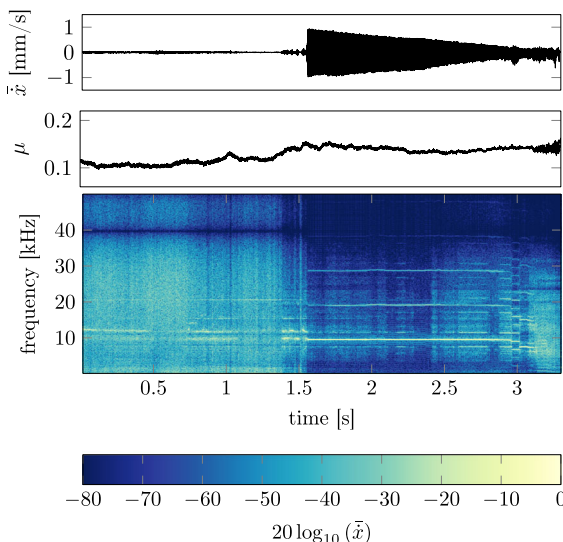


Fig. 5 Recorded time-series data for system III: normalized block velocity \bar{x} , friction coefficient μ and amplitude spectrogram of the velocity signal

with many higher harmonics. After $t = 3.13$ s, stick-slip oscillations are observed.

2.3 Signal analysis

Spectral analysis, that is (fast) Fourier transforms and related techniques, is a standard tool for signal analysis.

These methods rely on the stationarity assumption and linear superposition principle. The short-time Fourier transform allows to localize the frequency content of a signal in time. However, there are several other methods which are especially useful for analyzing complex non-stationary data from nonlinear systems, which are discussed hereafter. We introduce these techniques briefly in the following.

2.3.1 Orbit diagram

Nonlinear structural dynamics are typically studied in bifurcation diagrams, which depict the qualitative and quantitative evolution of the dynamics as a function of a control parameter. When dealing with measurement data, one can study the dynamics along time analogously to a bifurcation diagram. As we can only observe stable solutions and their transients, the exact notation of a bifurcation diagram may fall short for experimental data. Hence, the term 'orbit diagram' was introduced [26–29] as a generalized Poincaré section. The orbit diagram collects the amplitude of all local maxima of a time-series and displays them as dots along the time axis. From the evolution of the maxima, one can draw conclusions about the underlying dynamics and transitions: N co-existing bands of points represent period- N -limit cycles whereas unordered clouds of points stem from stochastic or chaotic data. Therefore, orbit diagrams allow for a simple and quick analysis of complex vibration data.

2.3.2 Nonlinear time-series analysis: the embedding theorem

In measurements, the data acquisition is often limited to very few measurement points. Hence, only a fraction of all active degrees of freedom of a given system can be measured. Takens' embedding theorem [30] enables to reconstruct all active degrees of freedom from a single univariate time-series measurement $s(t_1, \dots, \hat{t}_n)$. The $n = 1, \dots, \hat{n} - (m - 1)\tau$ state vectors in the m -dimensional reconstructed phase space are computed according to

$$\mathbf{q}_n = [s_{n-(m-1)\tau}, s_{n-(m-2)\tau}, \dots, s_{n-\tau}, s_n]^T, \quad (1)$$

where τ denotes the delay value. For strictly deterministic processes, the reconstructed attractor has the same geometrical and dynamical invariant measures

as the original invariant set in the true phase space. Hence, time delay embedding allows to draw conclusions about the qualitative and quantitative nature of the dynamical phase space computed from scalar time-series measurements [31,32]. Here, the embedding parameters τ and m are determined by the first minimum of the auto-mutual information function (AMI) [33] and vanishing fraction of false nearest neighbors (FNN) [34,35], respectively. Feeny and Liang [36] proposed to add the phase angle as additional delay coordinate to the reconstruction in order to avoid the collapse of the trajectories into the origin in the sticking phase. However, for reasons of consistency, we stick to the original embedding approach for the complete FIV range.

In order to increase the accuracy of the reconstruction, we apply an upsampling procedure to the measured signals. For upsampling to $f_s = 1\text{ MHz}$, we use spline interpolation with cubic characteristics.¹ This allows us to study approximately 100 points on the orbit of one period of the high-frequency FIV and thus detect dynamical transitions with high precision.

Furthermore, the reconstructed phase space is likely to have more than 3 dimensions, and it is thus impractical for visualization. Hence, principle component analysis (PCA) is used to compute the projection $\hat{\mathbf{q}}$ of the reconstructed trajectories \mathbf{q} onto the first $r = 3$ principle components of the phase space vectors to allow for a visual representation of the reconstructed attractor.

2.3.3 Recurrence plot quantification analysis (RPQA)

The recurrence plot (RP) [37,38] collects pairwise distances of points on trajectories \mathbf{q}_i in a phase space of a dynamical system. If the distance between two points on different trajectories is found to be small, these points are considered to recur to the same neighborhood in the phase space. Thresholding the matrix of all n pairwise distances yields the binary recurrence plot

$$\mathbf{R}_{i,j} = \Theta(\epsilon < |\mathbf{q}_i - \mathbf{q}_j|), \quad i, j \in 1, \dots, n. \quad (2)$$

Here, Θ denotes the heaviside function and ϵ represents the recurrence threshold, which decides on the neighborhood based on the distance between points i and j

¹ MATLAB interpolation command *interp1* with *spline* interpolation method.

in a given norm. To capture qualitative differences in RPs computed for different epochs of the measured signals, the recurrence threshold [39,40] is adjusted such that each RP exhibits a constant number of recurring points (fixed recurrence rate RR = 0.05). Trajectories that evolve parallel in time, such as in the case of a limit cycle, create parallel diagonal lines in the RP. On the other hand, intermittent dynamics create vertical line structures. Owing to the exponential divergence of nearby starting trajectories, the RP for chaotic systems is comprised of many short diagonal lines [41]. Recurrence plot quantification analysis (RPQA) enables the quantification of those line structures in the RP [42,43]. For this purpose, the probability distributions of line characteristics, such as length and vertical distance, are computed to define the RPQA metrics. In this work, we study the maximal diagonal and vertical line lengths, L_{\max} and V_{\max} , the average diagonal line length L and the determinism DET , which denotes the percentage of recurrence points forming diagonal lines. l_{\min} and v_{\min} denote the definition of the minimal length of a diagonal and vertical line, respectively. Furthermore, w_{Theiler} diagonals neighboring the main diagonal are discarded in the analysis. The recurrence time of second type, $T^{(2)}$, measures the average length of white vertical lines. The RPQA metrics can be used to describe and classify the dynamics encoded in the RP, and additionally facilitate time-series transition analysis. In this work, we employ RPQA to study qualitatively different dynamical regimes and detect dynamical transitions that are challenging to capture via spectral analysis [44]. Particularly, the RPQA metrics based on diagonal lines, e.g., DET , L_{\max} , and L detect chaos-order transitions, such as routes from regular dynamics to chaos. Chaos–chaos transitions become visible through the RPQA metrics that are computed from vertical line structure metrics, such as V_{\max} and $T^{(2)}$ [38,43,44].

2.3.4 Sliding window processing

The objective of this work is to study transitions of dynamics along time, i.e., along decreasing sliding velocity. Metrics are computed using a sliding window processing of the time-series input, i.e., metrics are computed for short successive time epochs separately. The window length is denoted by w and the hop size, that is the number of samples by which the window is shifted, is denoted by h . Hence, the overlap between two successive windows is given by $1 - h/w$.

The window size affects the range of dynamics that can be observed and must thus be chosen according to the time scales of interest. Short windows can detect instantaneous changes of high-frequency vibrations, while long windows can also capture slower dynamics. In most of the following discussions, we choose w such that approximately 10 high-frequency vibration cycles are captured within one window. For phase space reconstruction, the instantaneous embedding delay is computed for each window separately to capture the local temporal correlations that are present in the data. For the embedding dimension, a constant value is chosen throughout the complete time-series. This value is found by the maximal instantaneous dimension in a preceding study. This procedure ensures sufficiently high embedding dimensions for all sliding windows and allows for harmless over-embedding in regimes of lower-dimensional invariant sets.

3 Results

This work aims at illustrating various dynamic phenomena that were observed during the frictional tests corresponding to the systems I, II and III. We utilize the methods introduced before to study regular and irregular dynamics with special focus on transitions in sliding systems. Generally, the data and corresponding results are categorized into three regimes: *steady sliding* with small vibration amplitudes, *high-frequency* friction-induced vibrations of high amplitudes and *stick-slip* oscillations at low relative sliding velocity. Within each regime, relevant studies are conducted to illustrate the amount of information contained in a scalar time series recorded during the measurement.

3.1 Steady sliding in pre-FIV regime

As the three systems exhibit instability at different points in time, we introduce a generalized time in the range $[0, 1]$ that represents the steady sliding regime for each system such that we can depict qualitative behavior for all systems simultaneously.

3.1.1 Dominant setup mode at 105 Hz

In the first regime, all systems exhibit steady sliding with low vibration amplitudes. The spectral energy

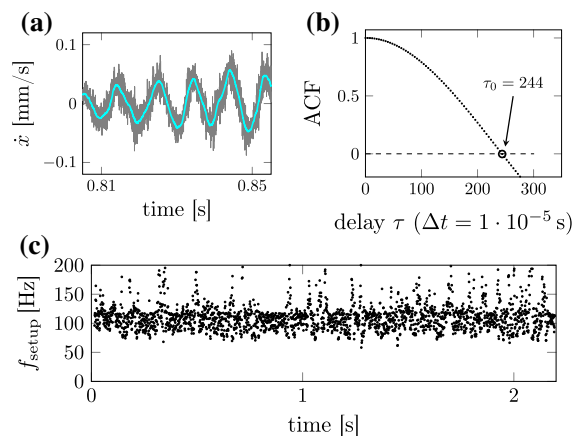


Fig. 6 Irregular fluctuations superimposed onto a low-frequency periodic motion: **a** 50-step moving average for a steady sliding segment from system I. The respective autocorrelation function in **b** indicates a-periodicity of $f_{\text{setup}} \approx 105 \text{ Hz}$ which can be attributed to an eigenfrequency of the experimental setup. **c** Depicts the evolution of this eigenfrequency for system I from start of measurement to onset of high-frequency FIV

covers a broad-banded frequency range with few pronounced peaks at the system's modes. A close view on the vibration signal reveals highly irregular fluctuations that are superimposed on a low-frequency periodic carrier oscillation, see Fig. 6a. Smoothing the data emphasizes the slow periodic motion which can be observed not only in the steady sliding, but also in the high-frequency FIV regime. To quantify this periodicity, we study the first zero τ_0 of the autocorrelation function ACF [45] of the filtered, i.e., smoothed, signal. The frequency is then given by $f_s / (4\tau_0)$. Sliding window processing ($w = 1000$, $h = 100$) of the ACF in the steady sliding regime indicates that this frequency is rather constant throughout the complete regime, see Fig. 6c. The analysis of the median frequency computed in this way reveals consistent values: 106.8 Hz (system I), 109.4 Hz (system II) and 104.6 Hz (system III). Hence, we assign this periodicity to an eigenfrequency f_{setup} of the complete experimental setup, which is excited during operation. The setup frequency presents in fact a bending mode of the loading structure at about 105 Hz.

3.1.2 Energy focusing behavior prior to instability

As the point of instability, i.e., the range of exponentially growing friction-induced vibrations, is approached, a reduction in the high-frequency fluctua-

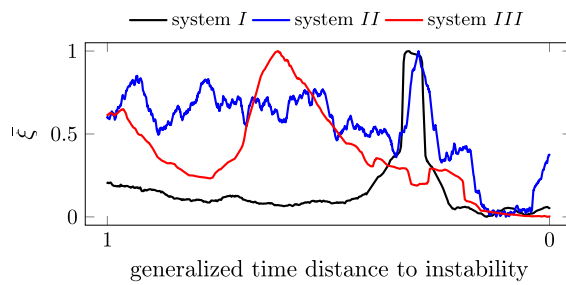


Fig. 7 Difference value ξ between filtered and raw signal (normalized to range $[0, 1]$) for all three systems along normalized time until the point of instability

tions about the main setup can be observed. We compute the root-mean square value of the absolute difference between the raw velocity signal \dot{x} and the filtered one \dot{x}_{smooth} (50-step moving average) for $n = 1 \dots w$

$$\xi = \sqrt{\frac{1}{w} \sum_{n=1}^w (\dot{x}_n - \dot{x}_{n,\text{smooth}})^2} \quad (3)$$

as a function of time (sliding window with $w = 10,000$, $h = 100$), cf. Fig. 7. As the point of instability is approached, this difference value decreases significantly. Hence, the vibration energy focuses in the setup mode around 105 Hz before the high-frequency FIV above 7 kHz set in. This behavior can be observed for all three systems under study, hence for different characteristics of the friction coefficient and different specimens. High peaks, as observed for system I, correspond to short epochs of high vibration level in the steady sliding regime (compare time signal in Fig. 3).

3.1.3 Attractor reconstruction

The embedding parameters τ and m are computed for the steady sliding regime along time to assess determinism and complexity of the vibration signal. The instantaneous delay value from the AMI is used to determine the embedding dimension. Here, the slow periodic trend is removed from the raw signal by subtraction of the moving-averaged (50 steps) trend as proposed in the previous section. No upsampling is applied to the data in this regime, since we cannot assume the dynamics to be strictly deterministic. Interpolation of this sequence would introduce determinism and therefore change the qualitative characteristic of the motion. Figure 8 displays the series of embedding parameters for system II

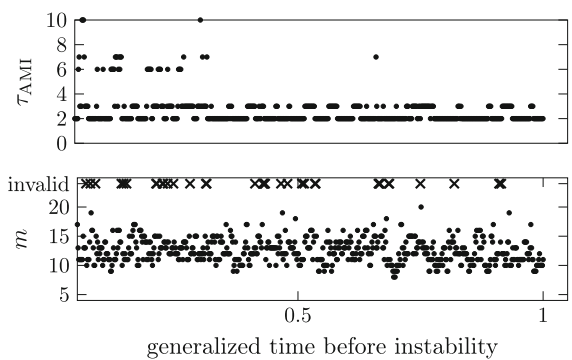


Fig. 8 Instantaneous embedding delay τ from auto-mutual information function and dimension m computed for the steady sliding regime of system II using a sliding window procedure ($w = 1000$, $h = 200$). Invalid m values represent epochs for which the fraction of FNN did not vanish within 20 dimensions

along time. To allow for a uniform illustration, the true time scale of the steady sliding regime is scaled to the generalized time.

Short temporal correlations are found by AMI values $2 \leq \tau \leq 4$, which indicates that successive values of the oscillation amplitude depend only on a few previous values. The instantaneous embedding dimension m exhibits values in the range of $8 \leq m \leq 20$. Hence, the reconstructed attractors are high-dimensional, but still deterministic. For some of the time epochs, the fraction of FNN does not vanish for $m = 20$ and is here displayed as *invalid* dimensions. Given the rather short epoch length of $w = 1000$, those invalid epochs represent only weakly deterministic or stochastic dynamics [21]. Similar results are obtained for systems II and III. In conclusion, the dynamics observed in the steady sliding regime are deterministic in large phase space dimensions with stochastic contributions.

3.2 Transitions in FIV for system I

Figure 9 depicts the qualitatively different dynamics observed for system I in the range of steady sliding, instability, high-frequency FIV and stick-slip oscillations: Representative time-series epochs, the corresponding reconstructed phase spaces, recurrence plots as well as series of recurrence plot quantifiers are displayed. For each representation, the studied signal (upsampled to 1 MHz) is normalized to a unit maximum absolute amplitude to allow for a consistent study of characteristics and metrics.

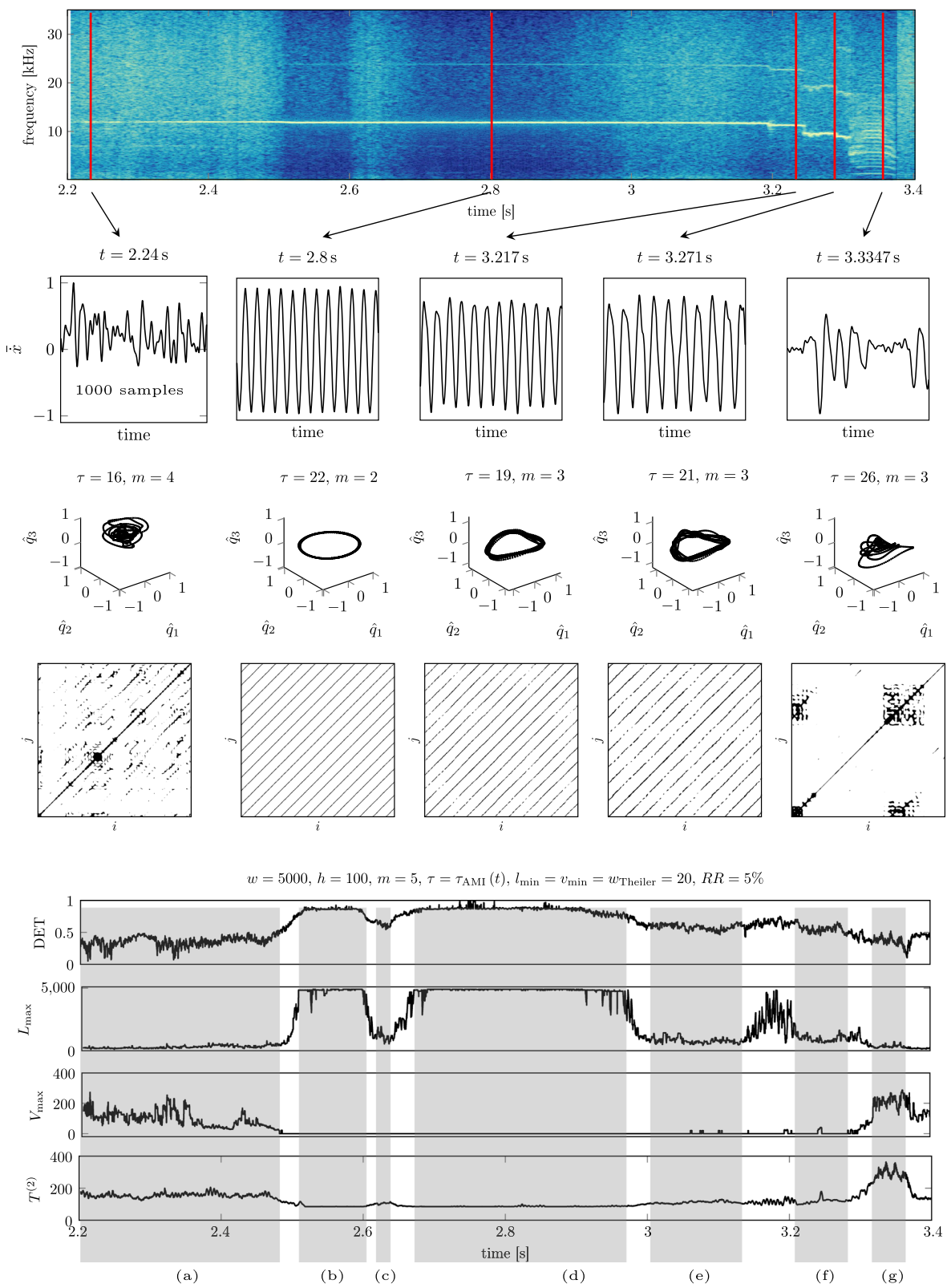


Fig. 9 Transitions in system I: spectrogram, selected time epochs, 3D PCA projection of the reconstructed attractor, the corresponding recurrence plot and series of RPQA metrics. See text for further details

Prior to high-frequency FIV, the time traces are highly irregular in segment (a): No distinct structure is formed by the trajectories in the reconstructed phase space. During high-frequency FIV ($t = 2.8\text{ s}$), the periodic time-series in segments (b) and (d) form a one-dimensional attractor, i.e., a limit cycle. At this point in time, the frequency spectrum is limited to the single vibration frequency at 11.9 kHz. The first jump in oscillation frequency happens at $t = 3.196\text{ s}$, after which the purely periodic character of the velocity signal is distorted slightly by amplitude modulations. The minimal embedding dimension increases to $m = 3$ and the attractor shows some deviations from a limit cycle in phase space. After the second frequency jump at $t = 3.245\text{ s}$, the signal is further distorted. The oscillation amplitude in positive direction modulates strongly, which creates a three-dimensional structure in the reconstructed phase space. At time point $t = 3.31\text{ s}$, the qualitative oscillation character changes to low-frequency stick-slip dynamics. The magnified time-series epoch from this regime illustrates the impulsive break-free phase and successive strongly damped oscillations that settle to zero before the next slip motion is initiated. The corresponding attractor has the form of a spiral that is also distorted in the third dimension. For the recurrence plot analysis, the embedding dimension is fixed to $m = 5$ throughout the complete signal, which represents the maximum of the instantaneous dimensions found in a preliminary study, reported in Fig. 17. Using a fixed recurrence rate of $\text{RR} = 0.05$, qualitatively different dynamics can be observed in the RPs for different signal stages: Before FIV, there are only a few line structures visible, which indicates weakly deterministic dynamics. The purely periodic motion is confirmed by long, non-interrupted diagonal lines in the corresponding RP. The vertical distance between these diagonal lines are constant and corresponds to the vibration period. The diagonal lines become interrupted in the two successive signal epochs due to the amplitude modulation of the vibration signal in segments (e) and (f). In the stick-slip phase (g), block-like structures are formed in the RP when the samples are sticking, which represents intermittent behavior in the reconstructed phase space.

The series of RPQA metrics quantifies the dynamics observed in the RPs. A larger window size $w = 5000$ was chosen to capture several stick-slip cycles and obtain qualitatively more robust quantifiers. DET and L_{\max} exhibit low values in the pre-FIV regime, which

corresponds to a high degree of irregularity. As FIV grow, the number of recurrence points forming diagonal lines growths and the resulting diagonal lines are longer. In the range $2.5 \leq t \leq 2.6\text{ s}$, almost all recurrence points form long diagonal lines, while no vertical lines can be observed. Hence, the dynamics in this regime form a regular period-1 limit cycle. At $t = 2.6\text{ s}$, DET and L_{\max} drop significantly without creating vertical lines. Hence, the recurrence plots still exhibit diagonal lines, but of distinctly smaller length. The RQA metrics are similar to the ones found after the frequency jumps at $t = 3.217$ and $t = 3.271\text{ s}$. In these regimes, the spectral energy is not as confined to a single frequency anymore, but spreads across a wider frequency range. Hence, the observed dynamics form a weakly chaotic attractor. The recurrence time of second type $T^{(2)}$ is rather constant throughout the FIV range and corresponds to the dominant periodicity of the oscillation frequency. The maximal vertical line length peaks at the time instants of frequency jumps. In the stick-slip regime, the diagonal lines are very short and vertical lines grow. Owing to the slower dynamics, the recurrence time increases in this section. Concluding, for this signal there are at least three qualitatively different dynamics which can be observed: regular period-1 limit cycle oscillations, low-dimensional irregular dynamics driven by small perturbations about a-periodic motion, and low-frequency stick-slip dynamics.

Figure 10 depicts a magnified view of the final range of the measurement with transitions from high-

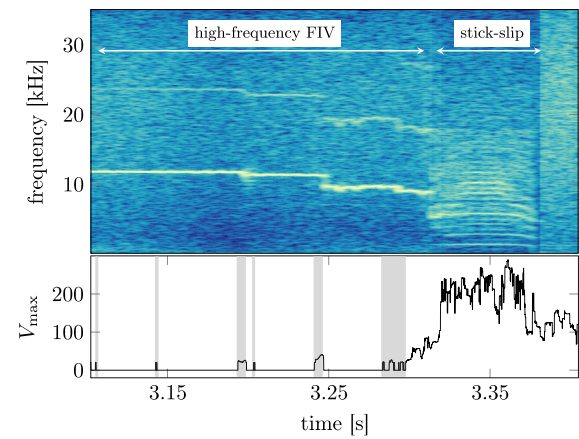


Fig. 10 Transitions from high-frequency vibrations over stick-slip oscillations to standstill in system I (detail view of Fig. 9). Spikes of the maximal vertical RP line length V_{\max} indicate short intermittent dynamics at dynamical transitions, $w = 1000$, $h = 100$, $v_{\min} = l_{\min} = w_{\text{Theiler}} = 20$, $\text{RR} = 5\%$

frequency FIV to stick-slip. Particularly, the RPQA metric V_{\max} indicates transitions in the dynamics by short spikes. During those sudden transitions, small block-type structures form in the RP and cause longer vertical lines. In the transition to the stick-slip regime, vertical lines grow rapidly. The intermittent dynamics during the sticking phase are clearly visible in this RPQA study, while V_{\max} values fall again in the zero-velocity limit toward standstill.

3.3 Transitions in FIV for system II

In contrast to system I, system II exhibits no stick-slip phase in the low sliding velocity range, see Fig. 11. In this system, the onset and first phase of the FIV are particularly notable. In the steady sliding regime, several modes are visible in the spectrum of the measurement signal. As FIV are growing, at least four modes (5.9, 6.5, 7.3 and 13.2 kHz) compete for the positive energy feedback in the system, which results in a-periodicity and beating phenomena. Finally, a period-2 limit cycle at 5.83 kHz is established at $t = 2.5$ s with four distinct higher harmonics at 11.64, 17.47, 23.29 and 29.11 kHz. Interestingly, the first harmonic at 11.6 kHz exhibits a higher spectral amplitude than the base frequency at 5.8 kHz. Since this system is self-excited, there is no clear notation of subharmonics to that one would address this phenomenon, which was also observed by Pilipchuk [20].

In the low velocity regime, FIV decay without further transitions to qualitatively different dynamics. The orbit diagram reveals the salient features of the dynamics measured for system II: low-frequency periodicities that correspond to the setup mode can be observed throughout the complete measurement. In the first regime of FIV up to $t = 2.5$ s, the maxima displayed in the orbit diagram show scattering behavior as a result of a-periodicity and beating. Then, the dynamics turn to the period-2 limit cycle, which creates two distinct bands of points in the orbit diagram. At low sliding velocities, FIV amplitudes decrease and the limit cycle oscillation smoothly turn into fluctuations about the low-frequency setup mode. The next discussion elaborates on the a-periodic regime in detail.

3.3.1 Beating phenomena in system II

The transition from steady sliding via a-periodic dynamics to a period-2 limit cycle is investigated in

detail using recurrence plot analysis, see Fig. 12. In the steady sliding regime, 5.88, 6.52, 7.28, 11.35, 11.72 (harmonic to 5.88 kHz) and 13.16 kHz show pronounced peaks in the spectrogram. At the onset of FIV, the 7.3 kHz contribution decreases, while the 11.3 kHz peak grows significantly. At this point in time, several distinct frequencies in the neighborhood of 11.3 kHz arise: peaks at 10.47, 10.89, 11.72 and 12.16 kHz become visible. In this frequency range, most of the spectral energy is confined. However, this pattern is also visible at half the frequency and at integer multiples of this lower frequency. Interestingly, the peak at 11.33 kHz carries the largest energy, i.e., shows the highest amplitude in the spectrum. The phenomenon of subharmonics is well-known in forced dynamical systems, where significant energy shares can also be observed at half the excitation frequency. However, in our case the system is purely self-excited, such that we cannot nominate a forcing frequency. Hence, this notion falls short for this type of systems. At $t = 2.478$ s, the pattern of five neighboring frequencies has spread slightly to lower frequency values due to a shift of the main peak to 11.25 kHz. However, the peak at 11.72 kHz remains constant and competes with the slightly lower frequency at 11.25 kHz. This scenario gives rise to the beating phenomenon which is clearly visible in the third time-series epochs shown. At time $t = 2.493$ s, the dynamics instantaneously turn to a period-2 limit cycle. At this point, the previously dominant frequency at 11.25 kHz has completely vanished, such that only harmonics of the 5.84 kHz frequency remain. Again, the spectral amplitude has the largest value at 11.72 kHz, while at first sight the spectrogram would propose to assign the resulting vibrations to a limit cycle oscillation at 5.84 kHz with at least four higher harmonics.

Time delay embedding enables the visualization of the underlying attractors. Before FIV onset, the invariant set is an irregular shape in the reconstructed phase space, which is also visible in the RP that exhibits many short diagonal lines. In the second time epoch, the attractor has a torus-like shape and the diagonal lines in the RP grow. The beating range exhibits a distinct structure in the phase space: the trajectories start to unfold the period-2 cycle through opening up the torus structure into the third dimension. Finally, the limit cycle oscillation is clearly visible in the phase space and the RP, which exhibits only long diagonal lines.

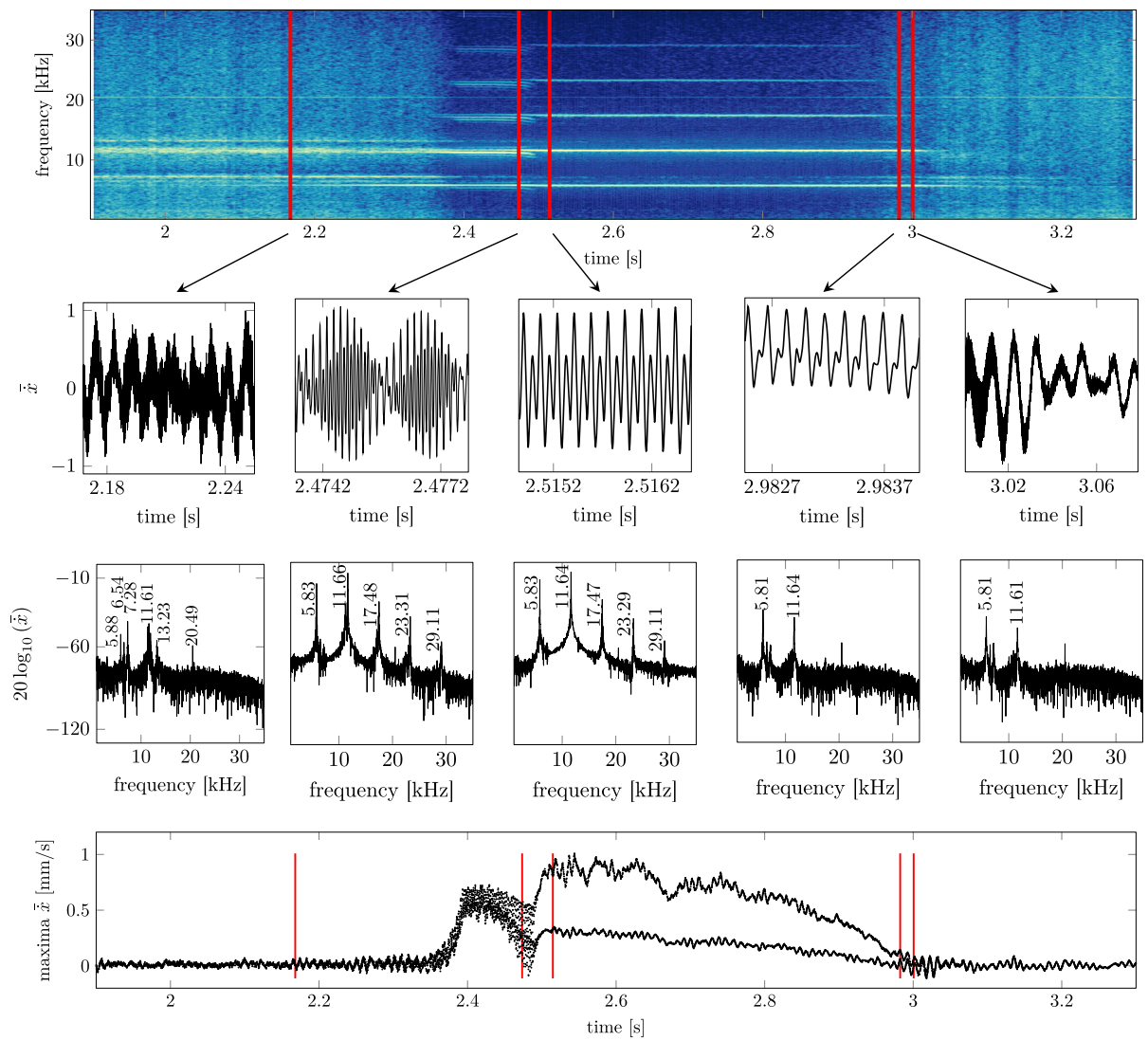


Fig. 11 Transitions in system II: spectrogram, selected time epochs (normalized amplitudes) with corresponding spectra ($n_{\text{FFT}} = 2^{14}$) and orbit diagram. See text for further details

The RQA measures L_{\max} , L and V_{\max} give further insight into the dynamical transitions. The maximal diagonal line length shows large values throughout the FIV range except for the time instants around $t = 2.48$ s, where the limit cycle is born out of the a-periodic beating-type dynamics. On the contrary, the maximal vertical line lengths increase during the beating phase and reveal a maximum right before the transition to the limit cycle vibration. The average diagonal line length exhibits small values throughout the pre-limit cycle regime. This indicates that neighboring trajectories on the underlying attractor evolve similarly

for only short times. In the limit cycle regime, the average diagonal line length increases to $L \approx 100$.

Concluding, the system II passes through qualitatively different dynamical regimes in the first segment of FIVs: First, the irregular trajectories settle to a torus-like structure with one dominant and several weaker frequencies. Then, two dominant vibration frequencies approach each other and give rise to transient beating phenomena, i.e., a-periodic dynamics on a complicated attractor. Through a sudden transition, a period-2 limit cycle is born.

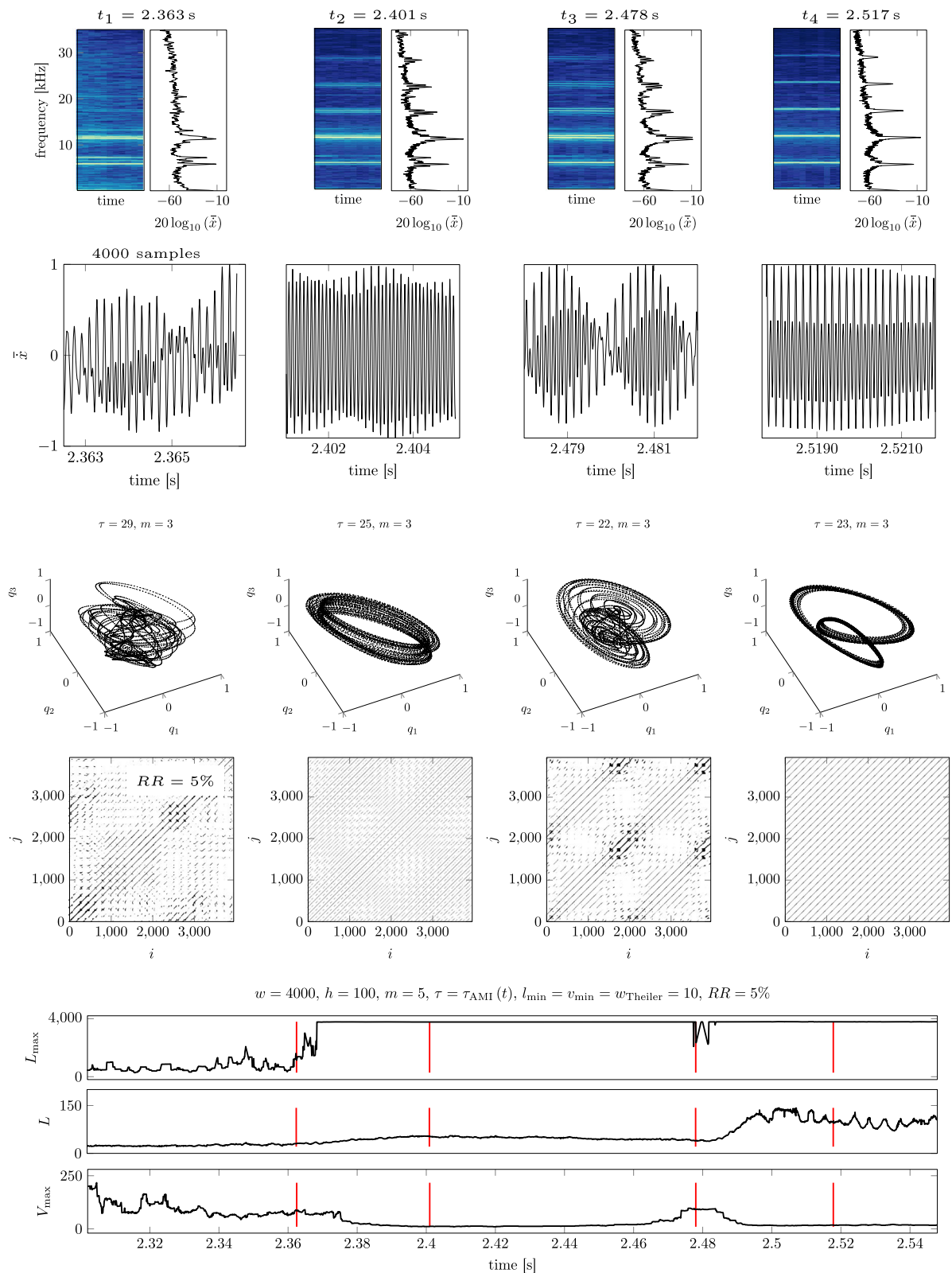


Fig. 12 A-periodic dynamics, beating behavior and birth of period-2 limit cycle oscillations in system II

3.4 Transitions in FIV for system III

System III exhibits a plethora of dynamical transitions, which are displayed in Fig. 13. FIV set in at $t = 1.56$ s and several transitions can be observed at $t = 2.95$ s, 3.01 s, 3.08 s and 3.26 s. In the first regime, the dominant vibration frequency is found at 9.62 kHz with two higher harmonics at 19.25 and 28.88 kHz. In the range $2.28 \leq t \leq 2.40$ s, there exists a window of purely periodic dynamics: the spectral energy is confined to this periodicity with vanishing broad-banded contents. The reconstructed attractor is an annular structure, i.e., a regular period-1 limit cycle. Time epochs before and after this periodic window show significantly broader spectra with significant energy shares throughout the complete frequency range. At $t = 2.92$ s, several periodicities appear at 7.57, 9.52 and 11.42 kHz. Shortly after, a sudden transition happens to a second periodic regime with at least 16 peaks in the spectrum, all of which corresponding to integer multiples of 2.29 kHz. Compared to the previous regime, only the 11.42 kHz periodicity recurs after the transition. Interestingly, the five highest spectral energies can be found at 9.13, 6.88, 16.01, 11.42 and 20.55 kHz (in descending order). A second transition happens at $t = 3.01$ s: Here, a 7.57 kHz frequency with three higher harmonics dominates the spectrum. In time domain, the signal is periodic with small amplitude modulations, which results in a RP with long diagonal lines. Due to a small kink at each peak in the positive value range, the reconstructed attractor forms a three-dimensional structure. From $t = 3.13$ s on, the system exhibits stick-slip vibrations.

For detecting and characterizing those transitions, the RPQA is particularly useful. The transition to more complex dynamics from the period-1 limit cycle regime is accompanied by a decrease of L_{\max} . In the second periodic window, the diagonal line lengths increase again. The maximal vertical line length indicates the transitions by single peaks. The onset of stick-slip vibrations, which are characterized by the laminar stick phase, is visible in V_{\max} . The following section elaborates further on the transition detection by means of RPQA.

3.4.1 Instantaneous vibration frequency jumps

Figure 14 depicts a magnified view into the various transitions happening in system III from high-

frequency FIV to stick-slip oscillations. In region (a), the limit cycle solution is indicated by long diagonal lines and vanishing vertical lines. Thus, trajectories in phase space evolve in parallel for long times and re-visit the same spatial regime periodically. Phase (b) is characterized by significantly shorter diagonal lines and no vertical lines, hence indicating chaotic dynamics. Successively, section (c) exhibits an increase in intermittent dynamics, i.e., vertical line structures, which indicates a chaos–chaos transition. At $t = 2.953$ s, V_{\max} peaks and L_{\max} has a minimum. These metrics indicate a short period of highly intermittent dynamics before diagonal line lengths grow quickly toward section (d). Here, diagonal lines exhibit a plateau of $L_{\max} \approx 1500$, which is a smaller value than in sections (a) and (e). Thus, the multiple harmonics and amplitude modulations render the dynamics quasi-periodic here. After a short chaotic transition, the system settles to more regular dynamics on an annular invariant set in (e) with vanishing vertical line structures and large L_{\max} values. Amplitude modulations, however, cause significantly shorter average lines than in section (a). The following transition through phase (f) represents the shift toward stick-slip vibrations in (g): diagonal line structures get very short and vertical lines growth quickly. The stick phases, i.e., small vibration velocity signals, represent the intermittent phase and cause long vertical lines. Concluding, system III exhibits rich, qualitatively different dynamics, that range from regular limit cycle oscillations over weakly chaotic motions to intermittent stick-slip vibrations. These results confirm previous results [20], which showed narrow bands of chaotic motion in numerical and experimental testings of frictional oscillators subjected to decreasing velocity profiles. In this work, the RPQA enhances the data-driven system characterization and transition detection.

3.5 Transition to stick-slip regime

The irregular transition from high-frequency FIV to stick-slip vibrations happens in system III at $t = 3.139$ s, see Fig. 15. In this regime, periodicities decrease and amplitudes modulate strongly, which has been confirmed by RPQA in Fig. 13. As the sliding velocity decreases further, stick-slip oscillations set in. Here, the upper block shows intermittent dynamics, i.e., periodic patterns of sticking phases and subsequent break-free oscillations. These oscillations persist for

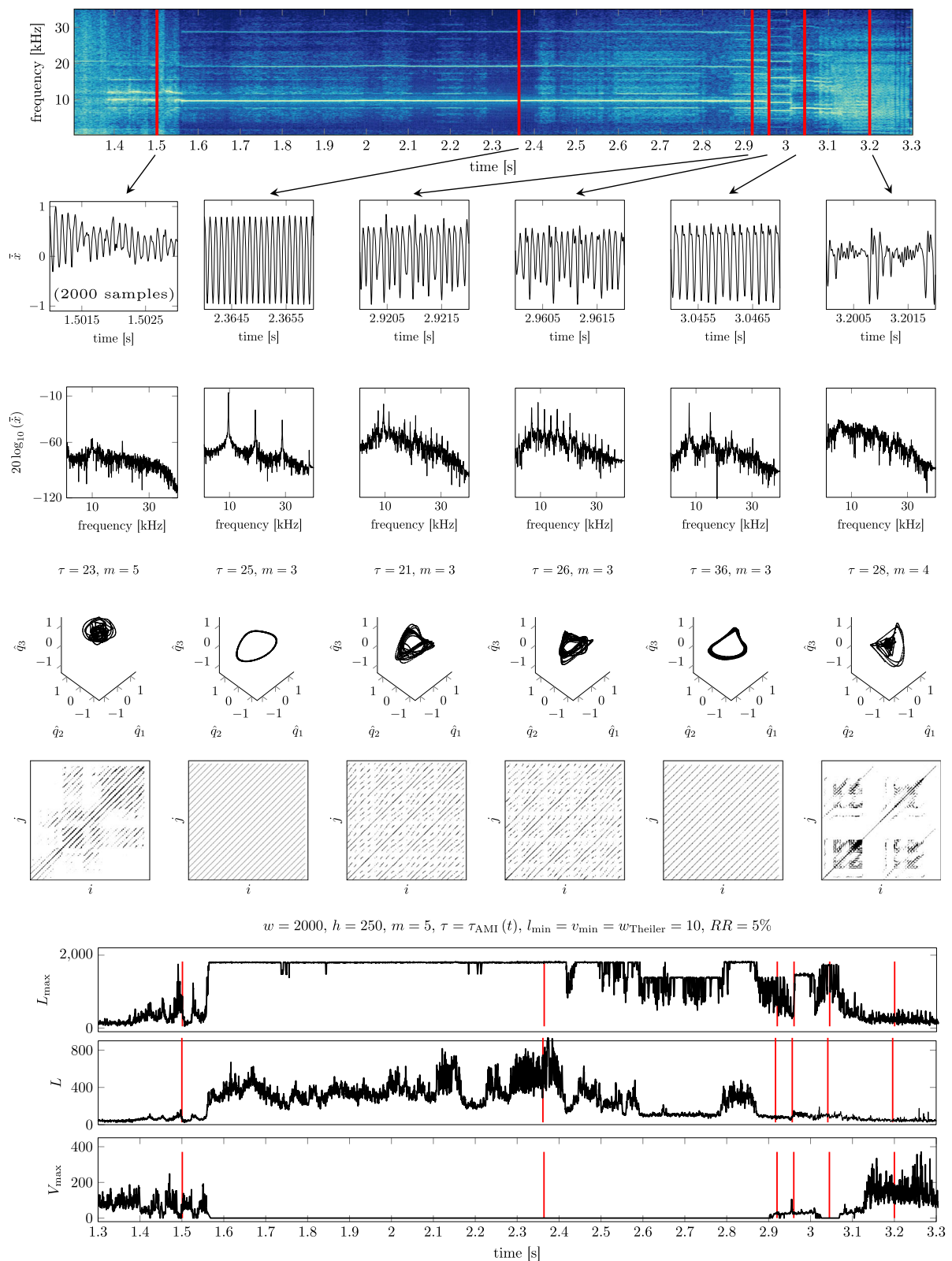


Fig. 13 Transitions in system III: spectrogram, selected time epochs (normalized amplitudes) with corresponding spectra ($n_{\text{FFT}} = 2^{11}$), reconstructed attractors and recurrence plot analysis. See text for further details

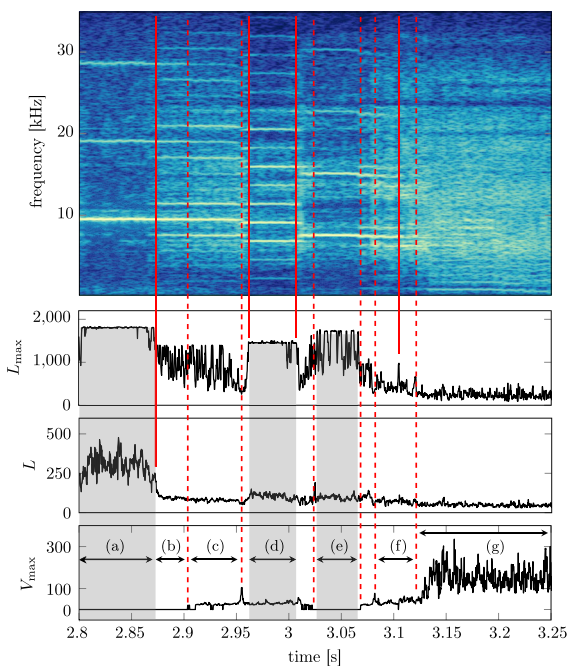


Fig. 14 Multiple transitions from regular to irregular and stick-slip vibrations in system III (detail view of Fig. 13): **a** regular period-1 limit cycle, **b** chaotic transition, **c** weakly chaotic regime, **d** quasi-periodic dynamics, **e** regular limit cycle, **f** chaotic transition, **g** intermittent stick-slip dynamics

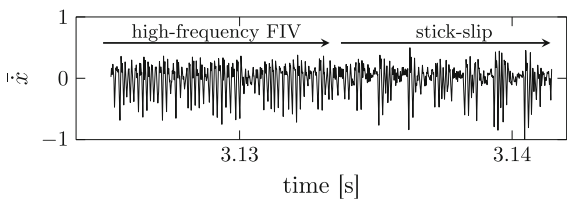


Fig. 15 Transition through irregular motion to self-excited stick-slip vibrations in system III

≈ 0.1 s until a second type of stick-slip cycles can be observed.

Shortly before standstill, at $t = 3.248$ s the stick-slip oscillations change their qualitative character. Up to this point, the vibrations are self-excited. After transition, the vibrations are induced periodically by the low-frequency setup mode, i.e., they turn to pseudo-forced stick-slip oscillations, see Fig. 16. After passing into the reverse vibration direction, the relative motion between the two blocks suffices to create short epochs of stick-slip motion, before the relative motion decays and annihilates the friction energy input from the interface.

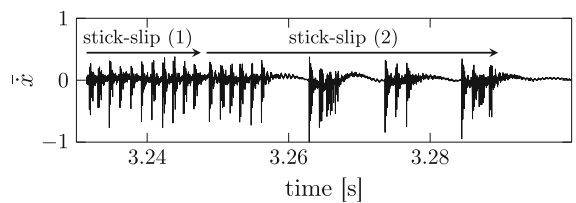


Fig. 16 Transition from self-excited stick-slip vibrations (1) to driven stick-slip motion (2) through the low-frequency setup mode in system III

4 Conclusion

Three vibration measurements from the frictional braking tests were studied by means of nonlinear time-series and recurrence plot analysis. Three elementary different dynamics were observed: steady sliding, high-frequency FIV and stick-slip vibrations at low sliding velocities. A slow setup mode at 105 Hz underlied the complete vibration signal and caused corresponding amplitude modulations. In the steady sliding regime, weakly deterministic dynamics with stochastic fluctuation were identified. The highly irregular fluctuations about the setup mode decay as the point of instability is approached. Hence, the energy absorbed from the friction interface localizes in the setup mode right before the dynamic instability. This behavior was observed for both a constant friction value and for a negative friction-velocity slope. The high-frequency FIV exhibited regular dynamics, i.e., motion on period-1 and period-2 limit cycles, in several cases. Spectral scatter, i.e., significant energy shares across the complete frequency range, rendered the limit cycle solutions weakly chaotic in some time epochs. Here, the RPQA enhanced the detection and dynamical characterization of the reconstructed attractors. At lower relative sliding velocities, two of the three signals exhibited sudden transitions in the dominant vibration periodicity due to a geometrical relaxation of the setup, or due to transitions to qualitatively different, i.e., chaotic, dynamics. Detailed time-series analysis revealed further transitions to stick-slip-type vibrations that exhibited intermittent dynamics at low sliding velocities. These results aim to provide a step forward on the application of nonlinear dynamics post-processing tools for identifying and characterizing the different frictional stable and unstable scenarios.

Acknowledgements M.S. was supported by the German Research Foundation (DFG) within the Priority Program 'calm, smooth, smart' under the reference Ho 3851/12-1. F.M. received

international visitor funds from the German Research Foundation (DFG) and the Priority Program 'calm, smooth, smart' to conduct parts of the research in this work.

Funding M.S. was supported by the German Research Foundation (DFG) within the Priority Program 'calm, smooth, smart' under the reference Ho 3851/12-1. F.M. received international visitor funds from the German Research Foundation (DFG) and the Priority Program 'calm, smooth, smart' to conduct parts of the research in this work.

Compliance with ethical standards

Conflict of interest The authors declare that they have no conflict of interest.

A Appendix

See Figs. 17, 18, 19

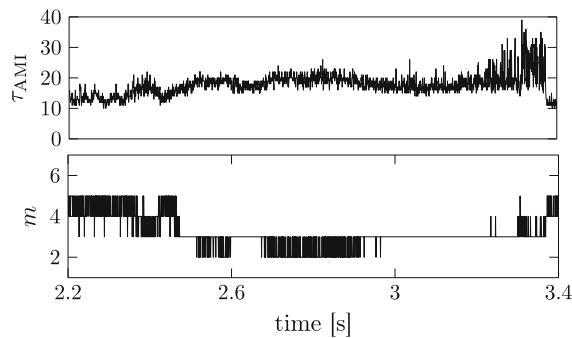


Fig. 17 Instantaneous embedding parameters computed using $w = 1000$ and $h = 500$ for system I

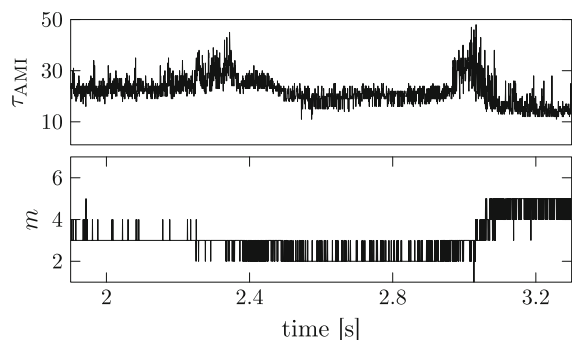


Fig. 18 Instantaneous embedding parameters computed using $w = 1000$ and $h = 500$ for system II

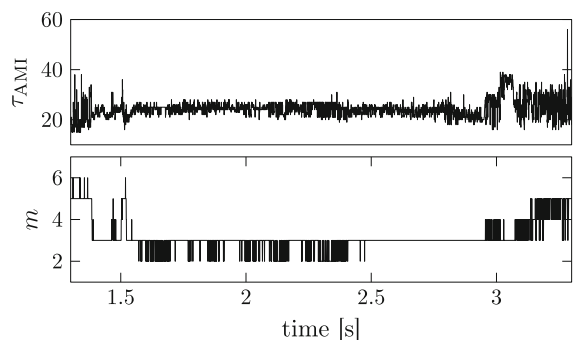


Fig. 19 Instantaneous embedding parameters computed using $w = 1000$ and $h = 500$ for system III

References

- Ibrahim, R.A.: Friction-induced vibration, chatter, squeal, and chaospert I. *Appl. Mech. Rev.* **47**(7), 209 (1994)
- Ibrahim, R.A.: Friction-induced vibration, chatter, squeal, and chaospert II. *Appl. Mech. Rev.* **47**(7), 227 (1994)
- Hoffmann, N., Fischer, M., Allgaier, R., Gaul, L.: A minimal model for studying properties of the mode-coupling type instability in friction induced oscillations. *Mech. Res. Commun.* **29**(4), 197–205 (2002)
- Sinou, J.J., Jzquel, L.: Mode coupling instability in friction-induced vibrations and its dependency on system parameters including damping. *Eur. J. Mech.—A/Solids* **26**(01), 106–122 (2007)
- Di Bartolomeo, M., Massi, F., Baillet, L., Culla, A., Fregolent, A.: Interplay between local frictional contact dynamics and global dynamics of a mechanical system. *Nonlinear Dyn.* **1**, 1–10 (2016)
- Gräßner, N., Tiedemann, M., von Wagner, U., Hoffmann, N.: Nonlinearities in Friction Brake NVH-Experimental and Numerical Studies. SAE International, Pittsburgh (2014)
- Kruse, S., Tiedemann, M., Zeumer, B., Reuss, P., Hetzler, H., Hoffmann, N.: The influence of joints on friction induced vibration in brake squeal. *J. Sound Vib.* **340**, 239–252 (2015)
- Lazzari, A., Tonazzi, D., Conidi, G., Malmassari, C., Cerutti, A., Massi, F.: Experimental evaluation of brake pad material propensity to stick-slip and groan noise emission. *Lubricants* **6**(4), 107 (2018)
- Feeny, B., Moon, F.C.: Chaos in a forced dry-friction oscillator. *J. Sound Vib.* **170**(3), 303–323 (1994)
- Ryabov, V.B., Ito, H.M.: Multistability and chaos in a spring-block model. *Phys. Rev. E* **52**(6), 6101–6112 (1995)
- Wiercigroch, M.: Chaotic vibration of a simple model of the machine tool-cutting process system. *J. Vib. Acoust.* **119**(3), 468 (1997)
- Awrejcewicz, J., Olejnik, P.: Stick-slip dynamics of a two-degree-of-freedom system. *Int. J. Bifurc. Chaos* **13**(04), 843–861 (2003)
- Pilipchuk, V.N., Tan, C.A.: CreepSlip capture as a possible source of squeal during decelerated sliding. *Nonlinear Dyn.* **35**(3), 259–285 (2004)

14. Gdaniec, P., Weiß, C., Hoffmann, N.: On chaotic friction induced vibration due to rate dependent friction. *Mech. Res. Commun.* **37**(1), 92–95 (2010)
15. Papangelo, A., Hoffmann, N., Grolet, A., Stender, M., Ciavarella, M.: Multiple spatially localized dynamical states in friction-excited oscillator chains. *J. Sound Vib.* **417**, 56–64 (2018)
16. Stender, M., Tiedemann, M., Hoffmann, N.: Characterization of complex states for friction-excited systems. *PAMM* **17**(1), 45–46 (2017)
17. Stender, M., Tiedemann, M., Hoffmann, N., Oberst, S.: Impact of an irregular friction formulation on dynamics of a minimal model for brake squeal. *Mech. Syst. Signal Process.* **107**, 439–451 (2018)
18. Popp, K., Stelter, P.: Stick-slip vibrations and chaos. *Philos. Trans. R. Soc. A Math. Phys. Eng. Sci.* **332**(1624), 89–105 (1990)
19. Pomeau, Y., Manneville, P.: Intermittent transition to turbulence in dissipative dynamical systems. *Commun. Math. Phys.* **74**(2), 189–197 (1980)
20. Pilipchuk, V., Olejnik, P., Awrejcewicz, J.: Transient friction-induced vibrations in a 2-DOF model of brakes. *J. Sound Vib.* **344**, 297–312 (2015)
21. Wernitz, B., Hoffmann, N.: Recurrence analysis and phase space reconstruction of irregular vibration in friction brakes. *J. Sound Vib.* **331**(16), 3887–3896 (2012)
22. Vitanov, N.K., Hoffmann, N., Wernitz, B.: Nonlinear time series analysis of vibration data from a friction brake. *Chaos Solitons Fractals* **69**, 90–99 (2014)
23. Oberst, S., Lai, J.: Chaos in brake squeal noise. *J. Sound Vib.* **330**(5), 955–975 (2011)
24. Oberst, S., Lai, J.: A statistical approach to estimate the Lyapunov spectrum in disc brake squeal. *J. Sound Vib.* **334**, 120–135 (2015)
25. Oberst, S., Lai, J.: Nonlinear transient and chaotic interactions in disc brake squeal. *J. Sound Vib.* **342**, 272–289 (2015)
26. Devaney, R.L., Eckmann, J.P.: An introduction to chaotic dynamical systems. *Phys. Today* **40**(7), 72 (1987)
27. Strogatz, S.H.: *Nonlinear Dynamics and Chaos: With Applications to Physics, Biology, Chemistry, and Engineering*. Mass, Cambridge (2001)
28. Peitgen, H.O., Jürgens, H., Saupe, D.: *Chaos and Fractals*. Springer, New York (2004)
29. Ross, C., Odell, M., Cremer, S.: The shadow-curves of the orbit diagram permeate the bifurcation diagram, too. *Int. J. Bifurc. Chaos* **19**(09), 3017–3031 (2009)
30. Takens, F.: Detecting Strange Attractors in Turbulence. *Dynamical Systems and Turbulence*, pp. 366–381. Springer, Berlin (1981)
31. Hegger, R., Kantz, H., Schreiber, T.: Practical implementation of nonlinear time series methods: the TISEAN package. *Chaos (Woodbury, N.Y.)* **9**(2), 413–435 (1999)
32. Kantz, H., Schreiber, T.: *Nonlinear Time Series Analysis*. Cambridge University Press, Cambridge (2003)
33. Fraser, A.M., Swinney, H.L.: Independent coordinates for strange attractors from mutual information. *Phys. Rev. A* **33**(2), 1134–1140 (1986)
34. Kennel, M.B., Brown, R., Abarbanel, H.D.I.: Determining embedding dimension for phase-space reconstruction using a geometrical construction. *Phys. Rev. A* **45**(6), 3403–3411 (1992)
35. Abarbanel, H.D.I., Brown, R., Sidorowich, J.J., Tsimring, L.S.: The analysis of observed chaotic data in physical systems. *Rev. Modern Phys.* **65**(4), 1331–1392 (1993)
36. Feeny, B.F., Liang, J.W.: Phase-space reconstructions and stick-slip. *Nonlinear Dyn.* **13**(1), 39–57 (1997)
37. Eckmann, J.P., Kamphorst, S.O., Ruelle, D.: Recurrence plots of dynamical systems. *Europhys. Lett. (EPL)* **4**(9), 973–977 (1987)
38. Marwan, N., Romano, M.C., Thiel, M., Kurths, J.: Recurrence plots for the analysis of complex systems. *Phys. Rep.* **438**(5–6), 237–329 (2007)
39. Marwan, N.: How to avoid potential pitfalls in recurrence plot based data analysis. *Int. J. Bifurc. Chaos* **21**(04), 1003–1017 (2011)
40. Kraemer, K.H., von Donner, R., Heitzig, J., Marwan, N.: Recurrence threshold selection for obtaining robust recurrence characteristics in different embedding dimensions. *Chaos* **28**(08), 085720 (2018)
41. Gao, J., Cai, H.: On the structures and quantification of recurrence plots. *Phys. Lett. A* **270**(1–2), 75–87 (2000)
42. Zbilut, J.P., Webber, C.L.: Embeddings and delays as derived from quantification of recurrence plots. *Phys. Lett. A* **171**(3–4), 199–203 (1992)
43. Marwan, N., Wessel, N., Meyerfeldt, U., Schirdewan, A., Kurths, J.: Recurrence-plot-based measures of complexity and their application to heart-rate-variability data. *Phys. Rev. E Stat. Nonlinear Soft Matter Phys.* **66**(2 Pt 2), 026702 (2002)
44. Trulla, L.L., Giuliani, A., Zbilut, J.P., Webber, C.L.: Recurrence quantification analysis of the logistic equation with transients. *Phys. Lett. A* **223**(4), 255–260 (1996)
45. Broomhead, D.S., King, G.P.: Extracting qualitative dynamics from experimental data. *Phys. D Nonlinear Phenom.* **20**(2–3), 217–236 (1986)

Publisher's Note Springer Nature remains neutral with regard to jurisdictional claims in published maps and institutional affiliations.